

Structural and Physical Properties of Delocalized Mixed-Valent $[\text{Cp}^*\text{M}(\text{pentalene})\text{M}'\text{Cp}^*]^{n+}$ and $[\text{Cp}^*\text{M}(\text{indacene})\text{M}'\text{Cp}^*]^{n+}$ ($\text{M}, \text{M}' = \text{Fe}, \text{Co}, \text{Ni}; n = 0, 1, 2$) Complexes

Juan M. Manriquez,^{1a,b} Michael D. Ward,^{*,1a,c} William M. Reiff,^{*,1d}
Joseph C. Calabrese,^{1a} Nancy L. Jones,^{1a,e} Patrick J. Carroll,^{1f}
Emilio E. Bunel,^{1a} and Joel S. Miller^{*,1a,g}

Contribution No. 7148 from the Science & Engineering Laboratories, DuPont, Experimental Station, Wilmington, Delaware 19880-0328, and the Department of Chemistry, Northeastern University, Boston, Massachusetts 02115

Received January 3, 1995[⊗]

Abstract: The structural characterization and physical properties of $[\text{Cp}^*\text{M}(\text{pentalene})\text{M}'\text{Cp}^*]^{n+}$ ($\text{Cp}^* = \text{penta-methylcyclopentadiene}$; $\text{M}, \text{M}' = \text{Fe}, \text{Fe}$ (**1a**); Co, Co (**1b**); Ni, Ni (**1c**); Ru, Ru (**1d**); Fe, Ru (**1e**); Fe, Co (**1f**); $n = 0, 1, 2$) and $[\text{Cp}^*\text{M}(s\text{-indacene})\text{M}'\text{Cp}^*]^{n+}$ ($s = \text{symmetric}$) and $[\text{Cp}^*\text{M}(as\text{-indacene})\text{M}'\text{Cp}^*]^{n+}$ ($\text{M}, \text{M}' = \text{Fe}, \text{Fe}$ (**2a, 3a**); Co, Co (**2b, 3b**); Ni, Ni (**2c, 3c**); $n = 0, 1, 2$) ($as = \text{asymmetric}$) are reported. The local molecular structure of the organometallic complex does not change significantly with oxidation state; in all cases the Cp^*M moieties reside on opposite faces of the fused μ -bridging ring systems, reflecting the dominance of steric effects. These complexes generally exhibit behavior consistent with significant electronic interactions between metal centers, including large electrochemical potential separations between successive one-electron redox events, and for the mixed valent ($n = 1+$) complexes, intervalent charge transfer absorption bands. The magnetic susceptibility data are consistent with intramolecular ferromagnetic coupling of spins for **1a**²⁺ and **2c**²⁺ and antiferromagnetic coupling of spins for **1c**, **1c**²⁺, **1b**, **2b**, **1c**⁺, **2c**⁺, and **3c**⁺. In general, the paramagnetic complexes exhibit Curie–Weiss behavior, except for **2c** and **3c**, which possess singlet ground states and high spin excited states that are 0.036 and 0.056 eV (290 and 524 cm^{-1}) above the ground state, respectively. Mixed-valent **1a**⁺ and **2a**⁺ are fully detrapped on the Mössbauer time scale (*i.e.*, electron transfer rates $\geq 10^7 \text{ s}^{-1}$) above 1.5 K, consistent with a negligible energy barrier to intramolecular electron transfer or complete delocalization. The EPR spectra of **1a**⁺, **2a**⁺, and **1e**⁺ exhibit significantly reduced g -factor anisotropies and more intense spectral features at ambient temperature compared to $[\text{FeCp}^*_2]^{n+}$, implying intramolecular electron transfer rates $\geq 10^{10} \text{ s}^{-1}$.

Introduction

Bimetalloocene complexes represent a unique class of compounds that has received considerable attention, especially with regard to the electronic interaction between metal centers.² Most notably, the mixed valent forms of these complexes commonly exhibit low-energy absorptions that are attributed to intervalent charge transfer between the metal centers similar to the well-documented Cruetz–Taube ion and its derivatives.³ The extent of delocalization, which can be described in terms of the rate of intramolecular electron transfer between metal centers, clearly is a sensitive function of the local ligand environment in mixed-valence complexes and the structure of the crystalline lattice.⁴

The presence of electronic interactions between metallocene centers suggests the possibility of magnetic interactions in odd-electron systems, especially in light of observations of ferromagnetism in electron-transfer salts of tetracyanoethylene (TCNE) and decamethylferrocene⁵ (FeCp^*_2) or decamethylmanganocene (MnCp^*_2)^{6,7} and, more recently, the reaction product of bis(benzene)vanadium and TCNE.⁸ These observations prompted us to investigate multidecker complexes in which intra- and intermolecular electronic interactions between the metal centers might result in interesting magnetic properties.⁹ We therefore identified the μ -bridging ligands pentalene,

[⊗] Abstract published in *Advance ACS Abstracts*, May 1, 1995.

(1) (a) Du Pont. (b) Present address: Department of Chemistry, Universidad Technica, Federico Santa Maria, Valparaiso, Chile. (c) Present address: Department of Chemical Engineering and Material Science, University of Minnesota, Admudson Hall, 421 Washington Ave. SE, Minneapolis, MN 55455. (d) Northeastern University. (e) Present address: Department of Chemistry and Biochemistry, La Salle University, Philadelphia, PA 19141. (f) Department of Chemistry, University of Pennsylvania, Philadelphia, PA 19104-6323. (g) Present address: Department of Chemistry, University of Utah, Salt Lake City, UT 84112.

(2) (a) Hendrickson, D. N.; Kramer, J. A. *Inorg. Chem.* **1980**, *19*, 3330. Voegeli, R. H.; Kang, H. C.; Finke, R. G.; Boekelheide, V. *J. Am. Chem. Soc.* **1986**, *108*, 7010. Van Order, N., Jr.; Geiger, W. E.; Bitterwolf, T. E.; Rheingold, A. L. *J. Am. Chem. Soc.* **1987**, *109*, 5680. Sorai, M.; Nishimori, A.; Hendrickson, D. N.; Dong, T.-Y.; Cohn, M. J. *J. Am. Chem. Soc.* **1987**, *109*, 4266. (b) Brown, G. M.; Meyer, T. J.; Cowan, D. O.; LeVanda, C.; Kaufman, F.; Roling, P. V.; Rausch, M. D. *Inorg. Chem.* **1975**, *14*, 506. (c) LeVanda, C.; Bechgaard, K.; Cowan, D. O.; Rausch, M. D. *J. Am. Chem. Soc.* **1977**, *99*, 2964.

(3) Cruetz, C.; Taube, H. *J. Am. Chem. Soc.* **1969**, *91*, 3988.

(4) Webb, R. J.; Geib, S. J.; Staley, D. L.; Rheingold, A. L.; Hendrickson, D. N. *J. Am. Chem. Soc.* **1990**, *112*, 5031. Lowery, M. D.; Hammack, W. S.; Drickamer, H. G.; Hendrickson, D. N. *J. Am. Chem. Soc.* **1987**, *109*, 8019.

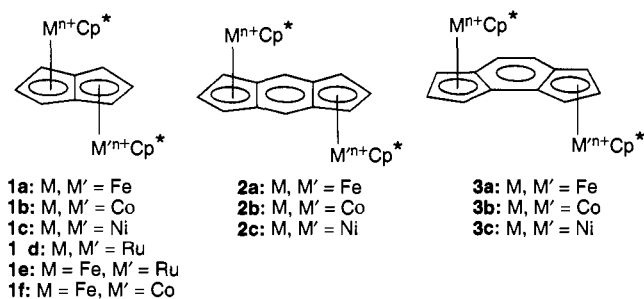
(5) Miller, J. S.; Epstein, A. J.; Reiff, W. M. *Chem. Rev.* **1988**, *88*, 201. Miller, J. S.; Epstein, A. J. *Chemtech* **1990**, *20*, 168. Miller, J. S.; Epstein, A. J.; Reiff, W. M. *Mol. Cryst., Liq. Cryst.*, **1985**, *120*, 27. Miller, J. S.; Calabrese, J. C.; Epstein, A. J.; Bigelow, R. W.; Zhang, J. H.; Reiff, W. M. *J. Chem. Soc., Chem. Commun.* **1986**, 1026.

(6) Broderick, W. E.; Thompson, J. A.; Day, E. P.; Hoffman, B. M. *Science* **1990**, *249*, 410.

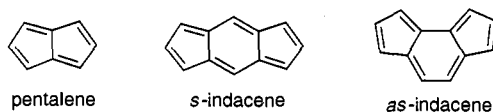
(7) Yee, G. T.; Manriquez, J. M.; Dixon, D. A.; McLean, R. S.; Groski, D. M.; Flippen, R. B.; Narayan, K. S.; Epstein, A. J.; Miller, J. S. *Adv. Mater.* **1991**, *3*, 309. Miller, J. S.; McLean, R. S.; Vazquez, C.; Yee, G. T.; Narayan, K. S.; Epstein, A. J. *J. Mat. Chem.* **1991**, *1*, 479.

(8) Manriquez, J. M.; Yee, G. T.; McLean, R. S.; Epstein, A. J.; Miller, J. S. *Science* **1991**, *252*, 1415. Epstein, A. J.; Miller, J. S. *Conjugated Polymers and Related Materials: The Interconnection of Chemical and Electronic Structure*; Proceedings of Nobel Symposium #NS-81; Salaneck, W. R., Lündstrom, I., Rånby, B., Eds.; Oxford University Press: Oxford, UK, 1993; p 475. Miller, J. S.; Yee, G. T.; Manriquez, J. M.; Epstein, A. J. *Ibid.*, p 461.

Chart 1



s-indacene, and *as*-indacene (*s* = symmetric; *as* = asymmetric)



as suitable choices for bridging metal ions. The corresponding bridged metallocene complexes **1–3** can be considered as the smallest subunits of extended metallocene polymers based on these ligands. We present herein the detailed physical and structural characterization of these complexes.

Experimental Section

Synthesis. All manipulations were carried out under an atmosphere of nitrogen using standard Schlenck techniques or in a Vacuum Atmospheres glovebox under nitrogen. Solvents used were predried and distilled from appropriate drying agents. The following compounds were prepared by literature methods: dihydropentalene,^{10a} *s*-indacene,^{10b} *as*-indacene,^{10c} Cp*M(acac) (M = Fe, Co, Ni),^{11a} and Cp*RuCl.^{11b} Compounds **1a–d**, **2a–c**, and **3a–c** were prepared by reacting 1 equiv of the dilithio salt of the appropriate ligand with 2 equiv of Cp*M(acac) (M = Fe, Co, Ni). Compound **1d** required the use of Cp*RuCl. Complexes **1e** and **1f** utilized the isolated intermediate Cp*Fe(pentalene) described below. Representative examples of the syntheses of the iron complexes are described below. The syntheses of the cobalt, nickel, and ruthenium analogs were accomplished using similar procedures. With the exception of **3c**²⁺, all compounds, some solvated, gave satisfactory elemental analysis. A complete summary of the product yields and elemental analyses is given in the supplementary material. Note that ¹H NMR data are not reported for paramagnetic complexes.

Cp*Fe(pentalene)FeCp* (1a). A solution of Fe(acac)₂ (7.33 g, 28.9 mmol) dissolved in THF (60 mL) was cooled to -78°C and added to a suspension of Cp*Li (4.10 g, 28.9 mmol) in THF (50 mL). The mixture was warmed to room temperature. A hexane solution of *n*-butyllithium (1.6 M, 18.9 mL, 30.3 mmol) was added dropwise to dihydropentalene (1.45 g, 14.5 mmol) dissolved in THF (40 mL) at -78°C forming dilithium pentalenide. The mixture was also warmed to room temperature. The Cp*Fe(acac) solution was added with stirring to the dilithium pentalenide solution at -78°C . The mixture was warmed to room temperature and stirred for 2 h. The solvent was removed in vacuo and the product was extracted with toluene until the extractions were colorless. The toluene extractions were combined and concentrated in vacuo until crystals were observed. Pentane was added and the solution cooled to -25°C overnight to give **1a** as black crystals in a 58% yield. Calcd elemental analysis for C₂₈H₃₆Fe₂: C, 69.44; H, 7.49. Found: C, 69.46; H, 7.42. ¹H NMR: δ CCH 3.89 (d, 4 H, 2.4 Hz), δ CHCHCH 3.13 (t, 2H, 2.4 Hz), and δ CH₃ 1.68 (s, 30 H).

Cp*Co(pentalene)CoCp* (1b). This complex was prepared in 63% yield in a manner identical to that used for **1a**. Calcd elemental analysis for C₂₈H₃₆Co₂: C, 68.57; H, 7.40. Found: C, 68.67; H, 7.39. ¹H

(9) Burdett, J. K.; Canadell, E. *Organometallics* **1985**, *4*, 805.

(10) (a) Katz, T. J.; Rosenberger, M.; O'Hara, R. K. *J. Am. Chem. Soc.* **1964**, *86*, 249. (b) Katz, T. J.; Balogh, V.; Schultman, J. *J. Am. Chem. Soc.* **1968**, *90*, 734. (c) Trogen, L.; Edlund, U. *Acta Chem. Scand.* **1979**, *B33*, 109.

(11) (a) Bunel, E. E.; Valle, L.; Manriquez, J. M. *Organometallics* **1985**, *4*, 1680. (b) Fagan, P. J.; Ward, M. D.; Calabrese, J. C. *J. Am. Chem. Soc.* **1989**, *111*, 1698.

NMR: δ CCH 2.92 (d, 4 H, 2.3 Hz), δ CHCHCH 5.86 (t, 2H, 2.3 Hz), and δ CH₃ 1.52 (s, 30 H).

Cp*Ni(pentalene)NiCp* (1c). This complex was prepared in 47% yield in a manner identical with that used for **1a**. Calcd elemental analysis for C₂₈H₃₆Ni₂: C, 68.64; H, 7.41. Found: C, 68.64; H, 7.41. ¹H NMR: δ CCH 3.33 (bs, 4 H), δ CHCHCH 3.20 (bs, 2H), and δ CH₃ 2.84 (s, 30 H).

Cp*Ru(pentalene)RuCp* (1d). This complex was prepared in 59% yield in a manner identical with that used for **1a**. Calcd elemental analysis for C₂₈H₃₆Ru₂: C, 58.52; H, 6.31. Found: C, 58.59; H, 6.36. ¹H NMR: δ CCH 4.28 (d, 4 H, 2.4 Hz), δ CHCHCH 3.95 (t, 2H, 2.4 Hz), and δ CH₃ 1.74 (s, 30 H).

Cp*Fe(pentalene)RuCp* (1e). Cp*RuCl (1.38 g, 5.09 mmol) was cooled to -78°C and treated with *n*-butyllithium (1.6 M, 3.2 mL, 5.09 mmol) in hexanes. The mixture was allowed to warm to room temperature. A solution of Fe(acac)₂ (1.33 g, 5.09 mmol) in THF (60 mL) cooled to -78°C was reacted with a suspension of Cp*Li (0.73 g, 5.09 mmol) in THF (80 mL) to generate in situ the lithio salt of Cp*Fe(pentalene). The mixture was warmed to room temperature. The solution containing the monolithiopentalene anion was added to the solution containing Cp*Fe(acac) (1.48 g, 5.09 mmol) at -78°C and the mixture was stirred at this temperature for 30 min and then allowed to warm to room temperature and stirred for 30 min. *n*-Butyllithium (1.6 M, 3.2 mL, 5.09 mmol) in hexanes was added via syringe to the solution containing Cp*Fe(pentalene) at -78°C . The mixture was allowed to warm to room temperature over a period of 15 min. The solution was recooled to -78°C and Cp*RuCl (1.38 g, 5.09 mmol) in 50 mL of THF was added. The mixture was allowed to warm to room temperature and then the solvent was removed in vacuo. The solid was extracted with hexane, the solution was filtered, and the solvent was stripped to dryness. Recrystallization of **1e** was accomplished from hexane with a yield of 1.44 g (53.3%). Calcd elemental analysis for C₂₈H₃₆FeRu: C, 63.51; H, 6.85. Found: C, 63.50; H, 6.87. The ¹H NMR for **1e**: δ CCH 4.31 (d, 2H, 2.2 Hz) and 3.83 (d, 2H, 2.2 Hz), δ CHCHCH 3.05 (t, 1H, 2.2 Hz) and 4.00 (t, 1H, 2.2 Hz), and δ CH₃ 1.68 (s, 30 H) and 1.71 (s, 15 H).

Cp*Fe(pentalene)CoCp* (1f). This complex was prepared in the same manner as **1e** using *n*-butyllithium (1.6 M, 2.8 mL, 4.48 mmol), Cp*Fe(pentalene) (1.3 g, 4.42 mmol), and Cp*Co(acac) (1.32 g, 4.51 mmol). The product was isolated from hexane (yield 1.3 g; 59.6%). Calcd elemental analysis for C₂₈H₃₆CoFe: C, 69.20; H, 7.45. Found: C, 68.99; H, 7.46.

[Cp*Fe(pentalene)FeCp*]²⁺[BF₄]⁻ (**1a**⁺). Cp*Fe(pentalene)FeCp* (150 mg, 0.31 mmol) dissolved in 20 mL of THF was added to [FeCp₂]²⁺[BF₄]⁻ (84 mg, 0.308 mmol) and the mixture was stirred at room temperature for 4 h resulting in the formation of a blue precipitate. The mixture was filtered and the insoluble material was washed with diethyl ether to remove all the ferrocene and dried in vacuo. The solid was recrystallized by slow diffusion of diethyl ether into a concentrated CH₂Cl₂ solution of **1a**⁺. Blue crystals (68%) were observed within 24 h. The crystals were filtered, washed with diethyl ether, and dried in vacuo. Calcd elemental analysis for C₂₈H₃₆BF₄Fe₂: C, 58.89; H, 6.35. Found: C, 58.53; H, 6.11.

[Cp*Fe(pentalene)FeCp*]²⁺{[BF₄]⁻}₂ (**1a**²⁺). [Cp*Fe(pentalene)FeCp*][BF₄]⁻ (150 mg, 0.263 mmol) dissolved in CH₂Cl₂ (20 mL) was added slowly to a CH₂Cl₂ (20 mL) solution containing 1,4-benzoquinone (30 mg, 0.28 mmol) and HBF₄·Et₂O (50 mg, 0.31 mmol). The mixture was stirred at room temperature for 0.5 h. Diethyl ether (20 mL) was added and the precipitate which formed was filtered, washed with diethyl ether, and then dried in vacuo. The solid was recrystallized by slow diffusion of diethyl ether into a concentrated acetonitrile solution of the complex. The black crystals (75%) were filtered, rinsed with diethyl ether, and dried in vacuo. Calcd elemental analysis for C₂₈H₃₆B₂F₈Fe₂: C, 51.12; H, 5.52. Found: C, 51.51; H, 5.51.

[Cp*Fe(*s*-indacene)FeCp*]²⁺ Complexes. The iron *s*-indacene analogs were prepared in the same manner as the pentalene complexes, using *s*-indacene. Cp*₂Fe₂(*s*-indacene), **2a**, was prepared in a 75% yield. Calcd elemental analysis for C₃₂H₃₈Fe₂: C, 71.93; H, 7.17. Found: C, 71.52; H, 7.51. ¹H NMR: δ CCHC 7.72 (s, 2H), δ CCHCH 4.68 (d, 4H, 3.5 Hz), δ CHCHCH 3.92 (t, 2H, 3.5 Hz), and δ CH₃ 1.55 (s, 30H). [Cp*₂Fe₂(*s*-indacene)][BF₄]⁻ (**2a**⁺) was prepared by reaction with [FeCp₂]²⁺[BF₄]⁻ in 70% yield. Calcd elemental analysis for C₃₂H₃₈BF₄Fe₂: C, 61.88; H, 6.17. Found: C, 62.23; H, 7.01. [Cp*₂

Table 1. Summary of Crystallographic Data for Cp*M(pentalene)M'Cp* and Cp*M(indacene)M'Cp* (M = Fe, Co, Ni) Compounds

	Cp* ₂ Co ₂ (pentalene) (1b)	[Cp* ₂ Fe ₂ (pentalene)] ⁺ [BF ₄] ⁻ (1a ⁺)	[Cp* ₂ Fe ₂ (s-indacene)] ⁺ [BF ₄] ⁻ (2a ⁺)	[Cp*Fe(pentalene)Cp*] ⁺ [BF ₄] ⁻	Cp* ₂ Ni ₂ (s-indacene) (2c)	[Cp* ₂ Ni ₂ (s-indacene)] ⁺ [BF ₄] ⁻ ·CH ₂ Cl ₂ (2c ⁺)	[Cp* ₂ Co ₂ (s-indacene)] ²⁺ {[BF ₄] ⁻ } ₂ (2b ²⁺)	Cp* ₂ Fe ₂ - (s-indacene) (2a)	Cp* ₂ Fe ₂ - (s-indacene) (3a)
formula	C ₂₈ H ₃₆ Co ₂	C ₂₈ H ₃₆ BF ₄ Fe ₂	C ₃₂ H ₃₈ BF ₄ Fe ₂	C ₂₈ H ₃₆ BF ₄ Fe	C ₃₂ H ₃₈ Ni ₂	C ₃₃ H ₄₀ BCl ₂ F ₄ Ni ₂	C ₃₂ H ₃₈ B ₂ Co ₂ F ₈	C ₃₂ H ₃₈ Fe ₂	C ₃₂ H ₃₈ Fe ₂
formula wt, daltons	490.46	571.11	621.17	515.26	540.08	711.82	714.14	534.35	534.35
color	black	black	black	dark green	black	black	dark red	dark green	dark red
cryst dimns, mm	0.46 × 0.20 × 0.49	0.45 × 0.15 × 0.45	0.50 × 0.21 × 0.46	0.32 × 0.05 × 0.48	0.37 × 0.07 × 0.40	0.27 × 0.07 × 0.48	0.42 × 0.44 × 0.48		
radiation	Mo Kα	Mo Kα	Mo Kα	Mo Kα	Mo Kα	Mo Kα	Mo Kα	Mo Kα	Mo Kα
temp, °C	-70	-70	-70	-70	-70	-70	-70	RT	RT
space group	P1̄ (no. 2)	P1̄ (No. 2)	P1̄ (No. 2)	P2 ₁ /c (No. 14)	P1̄ (No. 2)	C2/c (No. 15)	P2 ₁ /n (No. 14)	P1̄ (No. 2)	P2 ₁ /c (No. 14)
a, Å	8.479(2)	11.906(3)	8.587(1)	11.712(3)	7.402(2)	35.650(10)	7.953(2)	7.997(2)	8.149(2)
b, Å	11.270(2)	16.004(3)	11.446(1)	19.612(3)	8.0602(2)	9.027(1)	15.781(2)	8.341(2)	14.985(2)
c, Å	13.444(3)	16.288(2)	16.059(2)	11.642(3)	12.139(2)	22.617(3)	25.302(6)	11.677(2)	11.486(2)
α, deg	67.61(1)	68.70(1)	92.25(1)	90	85.27(2)	90.00	90.00	75.16(2)	90.00
β, deg	83.89(2)	75.25(2)	102.77(1)	104.40(1)	74.20(1)	114.66(1)	95.33(1)	72.70(2)	106.98(1)
γ, deg	83.74(2)	81.62(2)	107.89(1)	90	70.67(2)	90.00	90.00	64.88(2)	90.00
V, Å ³	1177.8	2601.5	1455.1	2565.3	656.9	6614.6	3161.8	665.7	1341.5
Z	2	4	2	4	1	8	2	1	2
density, g/cm ³	1.383	1.458	1.418	1.334	1.365	1.429	1.500	1.333	1.323
μ, cm ⁻¹	14.18	11.57	10.41	6.28	14.57	13.5	11.14	11.06	10.98
scan type	ω	ω	ω	ω	ω	ω	ω	ω-2θ	ω-2θ
scan rate, deg/min	1.70-5.00 (ω)	1.70-5.00 (ω)	1.70-5.00 (ω)	1.50-4.00 (ω)	1.8-4.00 (ω)	1.7-5.00 (ω)	1.5-5.00 (ω)	1.4-1.67 (ω)	1.4-1.67 (ω)
scan width, deg	1.20-1.90 ω	1.20-1.90 ω	1.20-1.90 ω	1.2-1.90 ω	1.20-1.90 ω	1.2-1.80 ω	1.20-1.90 ω	1.05 + 0.35(tanθ)	1.05 + 0.35(tanθ)
peak width at half-height, ω, deg	0.19	0.18	0.20	0.13	0.18	0.16	0.16		
2θ range, deg	3.3-52.0	2.7-50.0	2.6-52.0	2.1-52.0	3.5-60.0	2.0-52.0	1.6-55.0	4-55.0	4-50.0
relcns meas	4828/2623	9972/4430	5901/3475	5446/2320	3984/2525	7086/2919	7659/5013	3202/3051	2642/2356
(total/unique)									
solution method	Patterson method	direct methods	Patterson method	Patterson method	Patterson method	Patterson method	direct methods (SHELXS)	Patterson method	Patterson method
Hydrogen atoms	fixed	fixed	fixed	fixed	fixed	fixed	fixed	fixed	fixed
refinement	a	a	a	a	a	a	a	a	a
minimization function	Σw(F _o - F _c) ²	Σw(F _o - F _c) ²	Σw(F _o - F _c) ²	Σw(F _o - F _c) ²	Σw(F _o - F _c) ²	Σw(F _o - F _c) ²	Σw(F _o - F _c) ²	Σw(F _o - F _c) ²	Σw(F _o - F _c) ²
weighing scheme	α[σ ² (I) + 0.00091 ²] ^{1/2}	α[σ ² (I) + 0.00091 ²] ^{1/2}	α[σ ² (I) + 0.00091 ²] ^{1/2}	α[σ ² (I) + 0.00091 ²] ^{1/2}	α[σ ² (I) + 0.00091 ²] ^{1/2}	α[σ ² (I) + 0.00091 ²] ^{1/2}	α[σ ² (I) + 0.00091 ²] ^{1/2}	1/σ ² (I)	1/σ ² (I)
no. of parameters refined	271	631	352	307	208	379	397	154	163
data/parameter ratio	9.68	7.02	9.87	7.55	12.14	7.56	12.63	14.6	10.9
unweighted agreement factor, R	0.042	0.048	0.058	0.062	0.061	0.067	0.047	0.064	0.056
weighted agreement factor, R _w	0.047	0.042	0.056	0.056	0.074	0.049	0.056	0.079	0.070
high peak in final difference map, e ⁻ /Å ³	0.48 (Co2)	0.35 (C15)	0.50 (C10'-C14')	0.69 (F11)	0.84 (Ni1)	0.83 (Ni1)	0.75 (F13)	0.70 (C9)	0.46 (Fe)
diffractometer	CAD4	CAD4	CAD4	CAD4	CAD4	CAD4	CAD4	CAD4	CAD4

^a Full-matrix least-squares.

Table 2. Redox Potentials for Cp*₂M₂(pentalene) and Cp*₂M₂(indacene) Complexes

compd	THF			CH ₂ Cl ₂		
	E°(0/1+) ^b	E°(1/+2+) ^b	ΔE (V)	E°(0/1+) ^b	E°(1/+2+) ^b	ΔE (V)
Cp* ₂ Fe ₂ (pentalene), 1a	-0.61	0.24	0.85	-0.75	0.28	1.03
Cp* ₂ Co ₂ (pentalene), 1b	-1.35	-0.64	0.71	-1.49	-0.59	0.90
Cp* ₂ Ni ₂ (pentalene), 1c	-1.14	-0.49	0.65	-1.27	-0.41	0.86
Cp* ₂ Ru ₂ (pentalene), 1d	-0.19	0.10 ^c	0.29	-0.32	0.18 ^c	0.50
Cp* ₂ FeRu(pentalene), 1e	-0.56	0.27 ^c	0.83	-0.61	0.40 ^c	1.01
Cp* ₂ FeCo(pentalene), 1f	-1.31	0.02	1.33	-1.34	0.11	1.45
Cp* ₂ Fe ₂ (<i>s</i> -indacene), ^a 2a				-0.93	-0.11	0.82
Cp* ₂ Co ₂ (<i>s</i> -indacene), ^a 2b				-1.13	-0.32	0.81
Cp* ₂ Ni ₂ (<i>s</i> -indacene), ^a 2c				-0.99	-0.42	0.57
Cp* ₂ Fe ₂ (<i>as</i> -indacene), ^a 3c				-0.29	0.19	0.48
Cp* ₂ Co ₂ (<i>as</i> -indacene), ^a 3b				-1.44	-0.98	0.46
Cp* ₂ Ni ₂ (<i>as</i> -indacene), ^a 3c				-0.86	-0.31	0.55

^a Values not recorded in THF. ^b V vs Ag/0.1 M AgNO₃: the potential of the V vs Ag/0.1 M AgNO₃ reference electrode is approximately 0.30 V positive of the potential of a SCE reference electrode. The redox potentials in the table can therefore be converted to V vs SCE by adding 0.30 V. ^c These oxidations were irreversible and the potentials represent E_{1/2} values.

Fe₂(*s*-indacene)][BF₄]⁻ (**2a**²⁺) was prepared in 73% yield. Calcd elemental analysis for C₃₂H₃₈B₂F₈Fe₂: C, 54.29; H, 5.41. Found: C, 54.74; H, 5.38. The cobalt and nickel *s*-indacene complexes **2b** and **3c** were prepared similarly. ¹H NMR for **2b**: δ CCHC 7.43 (s, 2H), δ CCHCH 3.87 (d, 4H, 4.3 Hz), δ CHCHCH 4.94 (t, 4H, 4.3 Hz), and δ CH₃ 1.55 (s, 30 H).

[Cp*Fe(*as*-indacene)FeCp*]ⁿ⁺ Complexes. The iron *as*-indacene analogs were prepared in the same manner as the pentalene complexes, using *as*-indacene. Cp*₂Fe₂(*as*-indacene) (**3a**) was prepared in 79% yield. Calcd elemental analysis for C₃₂H₃₈Fe₂: C, 71.93; H, 7.17. Found: C, 71.84; H, 7.05. ¹H NMR: δ HC=CH 6.81 (s, 2H), δ CCH 4.1 (m, 2H), δ CHCHCH 4.0 (m, 2H), δ CCCH 3.73 (m, 2H), and δ CH₃ 1.62 (s, 30H). [Cp*₂Fe₂(*as*-indacene)][BF₄]⁻ (**3a**⁺) was prepared in 96% yield. Calcd elemental analysis for C₃₂H₃₈BF₄Fe₂: C, 61.88; H, 6.17. Found: C, 61.83; H, 6.26. [Cp*₂Fe₂(*as*-indacene)][BF₄]₂⁻ (**3a**²⁺) was prepared in 76% yield. Calcd elemental analysis for C₃₂H₃₈B₂F₈Fe₂: C, 54.29; H, 5.41. Found: C, 49.76; H, 4.57. The cobalt and nickel *as*-indacene complexes **3b** and **3c** were prepared similarly.

X-ray Structure Determination. Crystals of Cp*₂Co₂(pentalene) were grown from hexane whereas crystals of Cp*₂Ni₂(*s*-indacene), Cp*₂Fe₂(*s*-indacene), and Cp*₂Fe₂(*as*-indacene) were grown from hexane or toluene. The monocation salts were grown by diethyl ether diffusion into dichloromethane solutions of the monocation salts. [Cp*₂Co₂(*s*-indacene)]²⁺[BF₄]₂⁻ was grown by diethyl ether diffusion into acetonitrile solutions of the dication salt. Cell constants and an orientation matrix for the data collection were obtained by the standard methods from 25 reflections at -70 °C (or in the cases of **2a** and **3a** at room temperature). Systematic absences and subsequent least-squares refinement were used to determine the space groups. During data collection the intensities of several representative reflections were measured as a check on crystal stability. Where there was a loss of intensity during data collection, an isotropic decay correction (<3%) was applied. Equivalent reflections were merged and only those for which (F_o)² > 3σ(F_o)² were included in the refinement, where σ(F_o)² is the standard deviation based on counting statistics. Data were also corrected for Lorentz and polarization factors. Absorption corrections were made only for Cp*₂Co₂(pentalene) and [Cp*₂Fe₂(pentalene)]⁺[BF₄]⁻. Crystallographic details are summarized in Table 1 and tables of the atomic coordinates, anisotropic thermal parameters, and bond angles are provided as supplementary material.

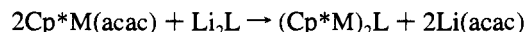
The structures of Cp*₂Co₂(pentalene), [Cp*₂Fe₂(*s*-indacene)]⁺[BF₄]⁻, Cp*₂Ni₂(*s*-indacene), [Cp*₂Ni₂(*s*-indacene)]⁺[BF₄]⁻·CH₂Cl₂, Cp*₂Fe₂(*s*-indacene), and Cp*₂Fe₂(*as*-indacene) were solved by automated Patterson analysis while the structures of [Cp*₂Fe₂(pentalene)]⁺[BF₄]⁻ and [Cp*₂Co₂(*s*-indacene)]²⁺[BF₄]₂⁻ were solved by direct methods, MULTAN and SHELEX, respectively. The hydrogen atoms were placed at calculated positions [(r(C-H) = 0.95 Å)]. All structures were refined by full-matrix least-squares of Σw[|F_o| - |F_c|]² with the neutral atom scattering factors taken from the literature.

Physical Characterization. Cyclic voltammetry was performed in an inert atmosphere drybox (Vacuum Atmospheres) with 0.1 M *n*-Bu₄N⁺ClO₄⁻/MeCN electrolyte in a conventional H-cell that included platinum working and auxiliary electrodes. Potentials were measured against a Ag/AgCl reference electrode in a 0.1 M AgNO₃ solution

separated from the working compartment by a porous Vycor plug. All potentials, *E*, are converted to values vs SCE. Voltammograms were recorded with a Princeton Applied Research (PAR) Model 173 potentiostat in conjunction with a PAR Model 175 programmer. UV-vis spectroscopic measurements were performed in either CH₂Cl₂ or CD₂Cl₂ solutions with a Cary 2300 spectrophotometer. Representative electronic absorption spectra (200 to 1400 nm) with nonabsorbing anions are presented as supplementary materials. Infrared spectroscopy was performed with Fluorolube or Nujol mulls between KBr plates with a Nicolet 7199 Fourier transform spectrophotometer. EPR spectra were recorded either on an IBM/Bruker ER 200 D-SRC or on a Bruker ER 420 spectrometer. Line positions were determined using field markers generated by an NMR gaussmeter while the microwave frequency was measured by a microwave frequency counter. ¹H NMR spectra were recorded on a GE/QE-300 spectrometer using benzene-d₆. Chemical shifts are reported in ppm relative to an external SiMe₄ standard. Zero-field Mössbauer spectra were acquired using a conventional constant acceleration spectrometer with a 50 mCi ⁵⁷Co source electroplated onto the surface and annealed into the body of the 6 μm thick foil of high purity rhodium in a hydrogen atmosphere. The details of this apparatus, including cryogenics and temperature control, have been described previously.¹² Magnetic susceptibility measurements were performed using the Faraday method in a Janis Supravariatemp variable-temperature cryostat as described previously.¹³

Results and Discussion

Chemistry. The reaction of Cp*M(acac) (M = Fe, Co, Ni or Ru), readily prepared from LiCp* and M(acac)₂, with Li₂L (L = pentalendiide, *s*-indacenediide, *as*-indacenediide) provides a convenient route to bridged metallocenes.^{11a,14} The primary advantages of this route are its simplicity, increased yields, and lack of unwanted side reactions.

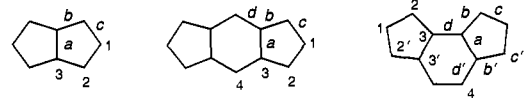


Cyclic voltammetry indicates that the pentalene and indacene compounds exhibit two successive one-electron transfers. The homometallic pentalene complexes **1a-d** exhibit large potential separations (ΔE) between successive events, with ΔE decreasing in the order **1a** > **1b** > **1c** > **1d** (Table 2). These large ΔE values are characteristic of strong electronic interaction between metal centers and extensive delocalization in the mixed-valent forms (*n* = 1) of these complexes. In all cases, the first oxidation occurs at more cathodic potential than the oxidation

(12) Cheng, C.; Reiff, W. M. *Inorg. Chem.* **1977**, *16*, 2097.

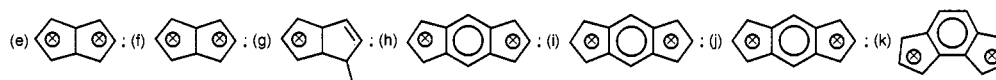
(13) Miller, J. S.; Dixon, D. A.; Calabrese, J. C.; Vazquez, C.; Krusic, P. J.; Ward, M. D.; Wasserman, E.; Harlow, R. L. *J. Am. Chem. Soc.* **1990**, *112*, 381.

(14) Bunel, E. E.; Campos, P.; Ruz, J.; Valle, L.; Chadwick, I.; Santa Ana, M.; Gonzalez, G.; Manriquez, J. M. *Organometallics* **1988**, *7*, 474. Bunel, E. E.; Valle, L.; Jones, N. L.; Carroll, P. J.; Gonzalez, M.; Munoz, N.; Manriquez, J. M. *Organometallics* **1988**, *7*, 789.

Table 3. Average Chemically Equivalent Bond Distances for Pentalene- and Indacene-Containing Compounds


	a	b	c	d	M-1 ^a	M-2	M-3	M-Cp* ^b	M-C ₅ ^c
Cp* ₂ Co ₂ (pentalene), 1b	1.432	1.425	1.439		1.977	2.048	2.284 ^e	1.684	1.724
[Cp* ₂ Fe ₂ (pentalene)] ¹⁺ , 1a⁺	1.496	1.440	1.413			2.035	2.093 ^f	1.670	1.652
Cp* ₂ Fe ₂ (<i>s</i> -indacene), 2a	1.458	1.437	1.410	1.396	2.036	2.046	2.133 ^j	2.025	1.731
[Cp* ₂ Fe ₂ (<i>s</i> -indacene)] ¹⁺ , 2a⁺	1.455	1.422	1.413	1.436		2.050 ⁱ		1.661	1.660 ^d
Cp* ₂ Ni ₂ (<i>s</i> -indacene), 2c	1.426	1.446	1.402	1.388	1.965	2.069	2.470 ^h	disordered	1.77 ^d
[Cp* ₂ Ni ₂ (<i>s</i> -indacene)] ¹⁺ , 2c⁺	1.411	1.435	1.414	1.390	1.973	2.062	2.346 ^h	1.71	1.764 ^d
[Cp* ₂ Co ₂ (<i>s</i> -indacene)] ²⁺ , 2b²⁺	1.457	1.444	1.406	1.401	2.033		2.122 ^j	1.640	1.671 ^d
Cp* ₂ Fe ₂ (<i>as</i> -indacene), 3a	1.414	1.426	1.426	1.467	2.016	2.034 ^k	2.064 ^j	1.643	1.647
	1.429	1.395	1.395		2.036	2.070		d	

^a Metal-carbon bond. ^b Metal-Cp* ring centroid distance. ^c Metal C₅-ring mean plane distance. ^d C₆-ring mean plane distance. ^{e-k} Structures e-f:



of the corresponding metallocene monomers, corroborating the stabilizing effect of the mixed-valent forms. This effect is much more dramatic than that observed for biferrrocene complexes,² suggesting greater delocalization in **1a-d**. The stability of the mixed-valent forms is readily apparent from the disproportionation constants, K_D , e.g., the K_D for **1a⁺** calculated from ΔE is 4×10^{-18} M. All the redox events are quasi-reversible, with the exception of **1d**. Reversible behavior for the **1d/1d⁺** redox couple is observed, but the second oxidation (**1d⁺/1d²⁺**) is not chemically reversible as evidenced by the lack of a return cathodic wave. This behavior is similar to that of RuCp*₂, which undergoes decomposition due to rapid loss of H⁺ from a methyl group following electrochemical oxidation.¹⁵ Apparently the stability of the mixed valent form, i.e., **1d⁺**, mitigates this event, as both Ru centers must be oxidized in order for this decomposition to take place.

Heterometallic complexes **1e** and **1f** also exhibit large separations between the 0/1+ and 1+/2+ redox waves, suggesting substantial delocalization of charge. The known electrochemical behavior of the iron and ruthenium metallocenes¹⁶ suggests that $E^\circ\{\mathbf{1e}/\mathbf{1e}^+\}$ is assignable to the Fe center initially [$E^\circ\{\text{Fe}(\text{C}_5\text{Me}_5)_2\}^{0/1+} = -0.12$ V vs SCE; $E^\circ\{\text{Fe}(\text{C}_5\text{H}_5)_2\}^{0/1+} = 0.41$ V], while $E^\circ\{\mathbf{1e}^+/\mathbf{1e}^{2+}\}$ can be assigned to the Ru center [$E^\circ\{\text{Ru}(\text{C}_5\text{Me}_5)_2\}^{0/1+} = 0.55$ V; $E^\circ\{\text{Ru}(\text{C}_5\text{H}_5)_2\}^{0/1+} = 0.88$ V]. The irreversibility of the second oxidation is similar to the behavior observed for RuCp*₂ which decomposes upon electrochemical oxidation.¹⁵ Similarly, the initial oxidation for $E^\circ\{\mathbf{1f}/\mathbf{1f}^+\}$ can be assigned to the cobalt center [$E^\circ\{\text{Co}(\text{C}_5\text{Me}_5)_2\}^{0/1+} = -1.47$ V; $E^\circ\{\text{Co}(\text{C}_5\text{H}_5)_2\}^{0/1+} = -0.91$ V]. The extremely large ΔE for **1f** suggests independent oxidation events at the metal centers, as it is unlikely that such large values would be realizable in intervalent complexes. However, Mössbauer data indicating an average iron environment for the monocation (*vide infra*) suggest substantial delocalization in **1e⁺**. Accordingly, the assignment of the electrochemical behavior to a mixed-valent state appears valid in this case. The data clearly reveal that, even in the heterometallic complexes, the redox properties of the metal centers are strongly influenced by each other. It also is important to note that the potential separations are always larger in CH₂Cl₂ than in THF, suggesting greater stability of the monocation of decreased stability of the dication in the former solvent.

The electrochemical properties of the *s*-indacene and *as*-indacene complexes **2a-c** and **3a-c** were investigated only in

CH₂Cl₂ due to their limited solubility in THF. In all cases, the compounds exhibited two quasi-reversible one-electron oxidations with large potential separations between events, characteristic of significant electronic interaction between metal centers. The potential separation is substantially greater for the *s*-indacene complexes, indicating greater electronic interaction in these complexes compared to the *as*-indacene analogs. The trends in the redox potentials are similar to those observed for the pentalene series, with $E^\circ\{0/1+\}$ increasing in the order Co < Ni < Fe. Similar trends are observed for $E^\circ\{1+/2+\}$ of the pentalene and *as*-indacene compounds, but for the *s*-indacene compounds the order is Ni < Co < Fe.

Crystal Structures. The single-crystal X-ray structures of the pentalene and *s*- and *as*-indacene complexes reveal that the Cp*M moieties reside on opposite faces of the fused μ -bridging ring systems, reflecting the dominance of steric effects. A similar geometry has been reported previously for [(CpFe)₂(μ_2 -C₅H₄)₂]^{17a} [I₃]⁻, [(C₅H₄Et)₂Fe₂(μ_2 -C₅H₄)₂FeC₅H₄CH₂Ph]^{17b} [I₃]⁻, and [(C₅H₄CH₂Ph)₂Fe₂(μ_2 -C₅H₄)₂Fe(C₅H₄CH₂Ph)]^{17c} [PF₆]⁻, but not for *N,N*-dimethyl-2,5''-(2-azonipropene-1,3-diyl)biferrrocenium pentafluoroborate.^{17d} For a given series of metal complexes for a particular ligand, the C-C bond distances do not differ appreciably (Table 3). The C-C bond lengths were consistent with values expected for the unsaturated ligand rings. The most significant difference among the complexes is the position of the metal atoms with respect to the ring [the position of the metal atoms with respect to the ligand rings as viewed normal to the ring planes is indicated by the symbol ⊗ in Table 3 and Scheme 1 (note that the Cp* ligand has been deleted for clarity)]. Most notable is the observation that the Ni atoms in **2c** and **2c⁺** are located near the outer position of the indacene rings, whereas the Fe atoms are located nearer the center. This may reflect the differences in the electron configuration of the two metals; the nickel complexes better satisfy the 18-electron rule by binding to the *s*-indacene ring in an η^3 -allyl manner. The mean plane distances differ for the different complexes;

(15) Kollé, U.; Grub, J. J. *Organomet. Chem.* **1985**, 289, 133.

(16) Ward, M. D. In *Electroanalytical Chemistry*; Bard, A. J., Ed.; Marcel Dekker: New York, NY 1989; p 181.

(17) (a) Cohn, M. J.; Dong, T.-Y.; Hendrickson, D. N.; Geib, S. J.; Rheingold, A. L. *J. Chem. Soc., Chem. Commun.* **1985**, 1095. (b) Dong, T.-Y.; Hendrickson, D. N.; Iwai, K.; Cohn, M. J.; Geib, S. J.; Rheingold, A. L.; Sano, H.; Motoyama, I.; Nakashima, S. *J. Am. Chem. Soc.* **1985**, 107, 7996. (c) Konno, M.; Sano, H. *Bull. Chem. Soc. Jpn.* **1988**, 61, 1455. (d) Webb, R. J.; Rheingold, A. L.; Geib, S. J.; Staley, D.; Hendrickson, D. N. *Angew. Chem., Int. Ed. Engl.* **1989**, 28, 1388. (d) Zhang, W.; Wilson, S. R.; Hendrickson, D. N. *Inorg. Chem.* **1989**, 28, 4160.

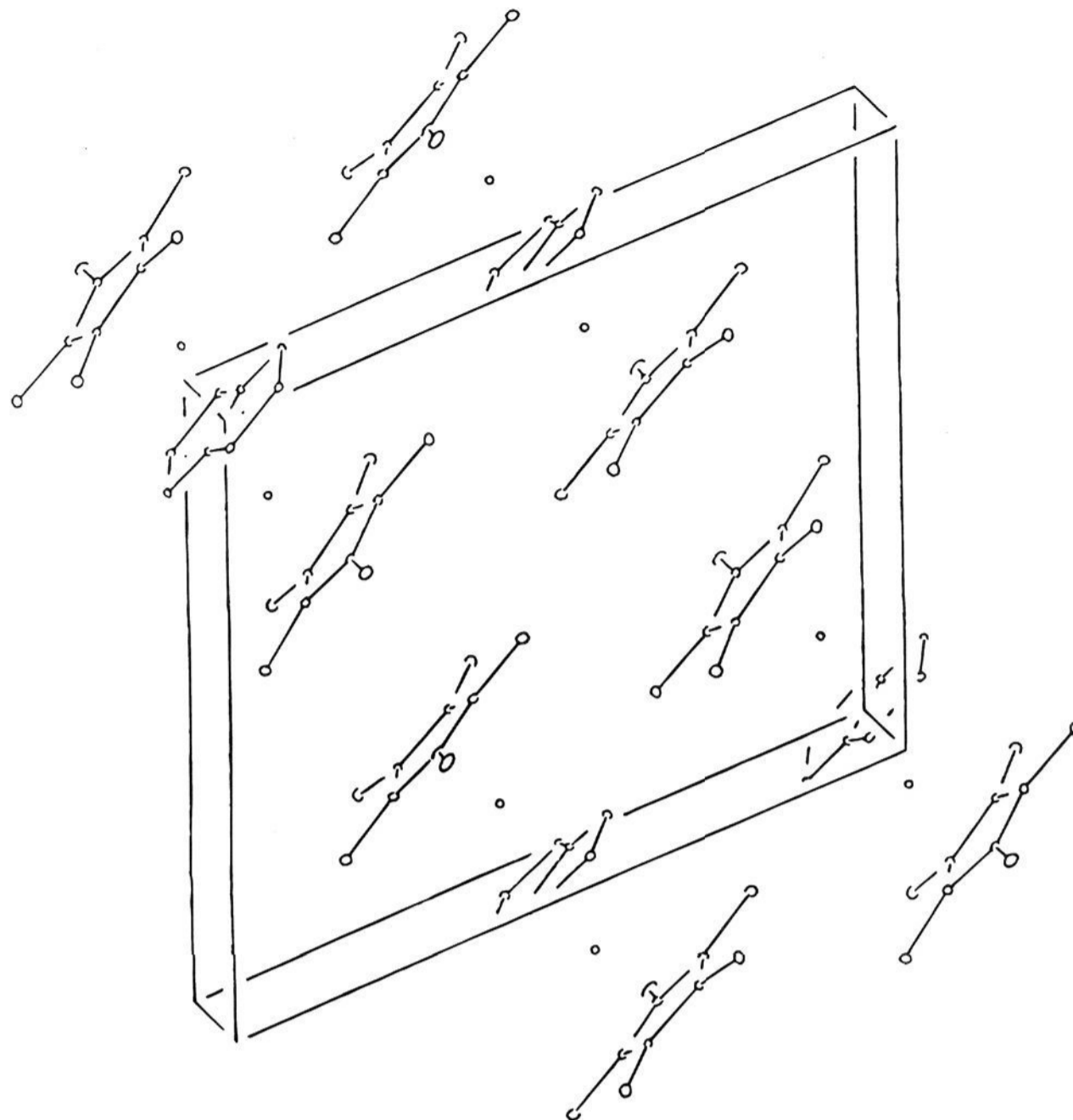


Figure 1. Stereoview of the unit cell showing the chain motif of $\text{Cp}^*_2\text{Co}_2(\text{pentalene})$ (**1a**).

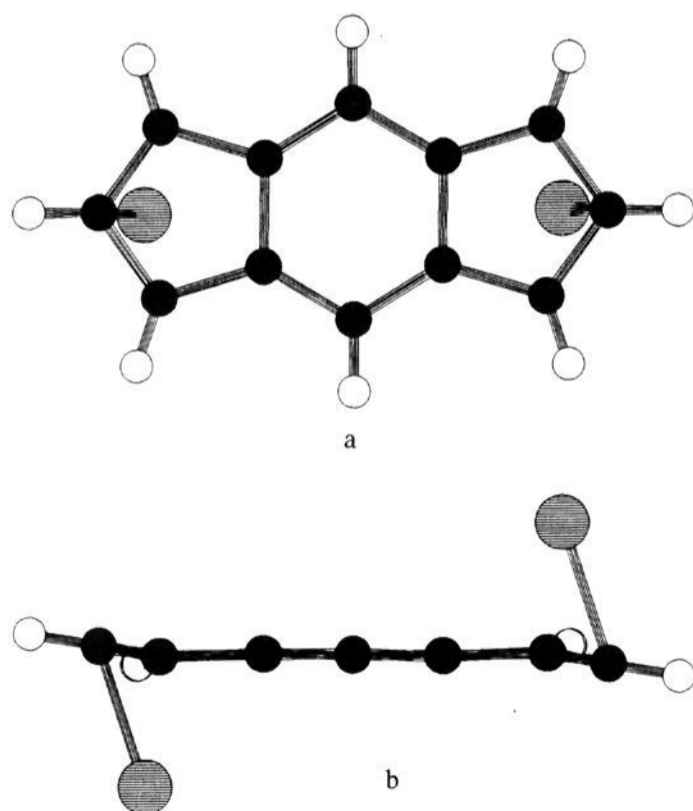


Figure 2. Short Ni-central C of the allyl moiety bonding in $\text{Cp}^*_2\text{Ni}_2(\text{s-indacene})$ (**3c**) (a) and nonplanarity of the indacene ligand (b).

however, because of the different position of the metal atoms it is difficult to evaluate the significance of these values.

The solid state structure of the complexes generally reveals packing of the molecules into chain-like structures (Figure 1). No unusual intermolecular distances are present. The intermolecular Cp^*-Cp^* interplanar separations within a chain typically exceed 3.5 Å. Thus, the crystalline materials can be described

Scheme 1

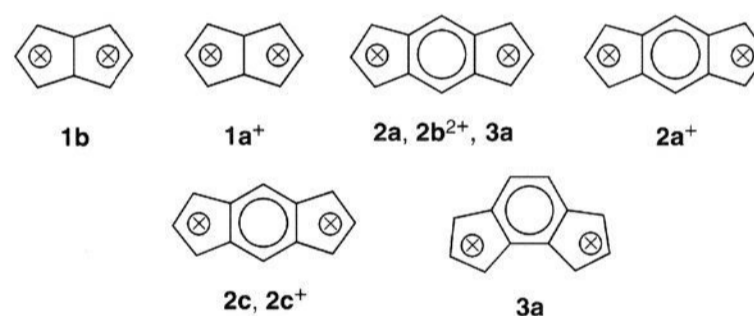


Table 4. Intervalent Transfer Absorption Bands for Mixed-valent $[\text{Cp}^*_2\text{M}_2(\text{pentalene})]^+$ Complexes

complex	λ_{max} (nm)	$h\nu_{\text{max}}$ (eV)	$h\nu_{\text{max}}$ (cm^{-1})	$\Delta h\nu_{1/2}$ (cm^{-1})	ϵ ($\text{M}^{-1} \text{cm}^{-1}$)
$[\text{Cp}^*_2\text{Fe}_2(\text{pentalene})]^{*+}$, 1a ⁺	2200	0.56	4543	2216	3470
$[\text{Cp}^*_2\text{Co}_2(\text{pentalene})]^{*+}$, 1b ⁺	1048	1.18	9542	1665	8400
$[\text{Cp}^*_2\text{Ni}_2(\text{pentalene})]^{*+}$, 1c ⁺	1007	1.23	9930	1600	420
$[\text{Cp}^*_2\text{Ru}_2(\text{pentalene})]^{*+}$, 1d ⁺	1219	1.02	8203	1746	1160
$[\text{Cp}^*_2\text{FeRu}(\text{pentalene})]^{*+}$, 1e ⁺	1258	0.99	7949	2153	275
$[\text{Cp}^*_2\text{FeCo}(\text{pentalene})]^{*+}$, 1f ⁺	1038	1.19	9634	2433	575
$[\text{Cp}^*_2\text{Fe}_2(\text{s-indacene})]^{*+}$, 2a ⁺	1885	0.65	5305	1587	2500
$[\text{Cp}^*_2\text{Co}_2(\text{s-indacene})]^{*+}$, 2b ⁺	1200	1.03	8333	1898	1690
$[\text{Cp}^*_2\text{Ni}_2(\text{s-indacene})]^{*+}$, 2c ⁺	1340	0.92	7463	1269	225

as ensembles of isolated molecules with negligible intermolecular interactions. This is consistent with the observed physical properties, which indicate the absence of cooperative interactions in the solid state (vide infra).

Electronic Absorption Spectra. The mixed-valent compounds **1a**⁺–**f**⁺ and **2a**⁺–**c**⁺ exhibit bands in the near-IR region that are reminiscent of intervalent charge-transfer absorptions commonly observed for mixed-valent compounds, Table 4.

Table 5. Magnetic Moments for Pentalene and Indacene Complexes^a

	no of spins per dimer	effective moment, $\mu_{\text{eff}}, \mu_B/\text{dimer}$	Curie-Weiss (CW) constant, θ , K
[Cp* ₂ Fe ₂ (pentalene)], 1a	0	diamagnetic	
[Cp* ₂ Fe ₂ (pentalene)] ⁺ [BF ₄] ⁻ , 1a⁺	1	2.11	-7.45
[Cp* ₂ Fe ₂ (pentalene)] ²⁺ {[BF ₄] ⁻ } ₂ , 1a²⁺	2	3.77	-12.16
[Cp* ₂ Co ₂ (pentalene)], 1b	0	diamagnetic	
[Cp* ₂ Co ₂ (pentalene)] ⁺ [BF ₄] ⁻ , 1b⁺	1	1.73	-4.01
[Cp* ₂ Co ₂ (pentalene)] ²⁺ {[BF ₄] ⁻ } ₂ , 1b²⁺	0	diamagnetic	
Cp* ₂ Ni ₂ (pentalene), 1c (not CW $T > 180$ K)	0	diamagnetic	
[Cp* ₂ Ni ₂ (pentalene)] ⁺ [BF ₄] ⁻ , 1c⁺	3	1.83	-3.50
[Cp* ₂ Ni ₂ (pentalene)] ²⁺ {[BF ₄] ⁻ } ₂ , 1c²⁺	0	diamagnetic	
Cp* ₂ FeCo(pentalene), 1f	1	1.79	-1.57
[Cp* ₂ FeCo(pentalene)] ⁺ [BF ₄] ⁻ , 1f⁺	0	diamagnetic	
[Cp* ₂ FeCo(pentalene)] ²⁺ {[BF ₄] ⁻ } ₂ , 1f²⁺	1	2.43	-38.9
[Cp* ₂ FeRu(pentalene)] ⁺ [BF ₄] ⁻ , 1e⁺	1	1.90	3.74
[Cp* ₂ Fe ₂ (<i>s</i> -indacene)], 2a	0	diamagnetic	
[Cp* ₂ Fe ₂ (<i>s</i> -indacene)] ⁺ [BF ₄] ⁻ , 2a⁺	1	1.91	-0.05
[Cp* ₂ Fe ₂ (<i>s</i> -indacene)] ²⁺ {[BF ₄] ⁻ } ₂ , 2a²⁺ (not CW)	2		
$T > 100$ K		2.84	-37
$T < 100$ K		2.34	-1.6
Cp* ₂ Co ₂ (<i>s</i> -indacene), 2b	0	diamagnetic	
[Cp* ₂ Co ₂ (<i>s</i> -indacene)] ⁺ [BF ₄] ⁻ , 2b⁺	1	1.62	-7.43
[Cp* ₂ Co ₂ (<i>s</i> -indacene)] ²⁺ {[BF ₄] ⁻ } ₂ , 2b²⁺	0	diamagnetic	
Cp* ₂ Ni ₂ (<i>s</i> -indacene), 2c (Not CW $T < \sim 115$ K)	4	2.90, 3.04	-72, -114
[Cp* ₂ Ni ₂ (<i>s</i> -indacene)] ⁺ [BF ₄] ⁻ , 2c⁺	3	1.69	-8.86
[Cp* ₂ Ni ₂ (<i>s</i> -indacene)] ²⁺ {[BF ₄] ⁻ } ₂ , 2c²⁺	2	2.01	-7.02
[Cp* ₂ Fe ₂ (<i>as</i> -indacene)], 3a	0	diamagnetic	
[Cp* ₂ Fe ₂ (<i>as</i> -indacene)] ⁺ [BF ₄] ⁻ , 3a⁺	1	2.49	-4.11
[Cp* ₂ Fe ₂ (<i>as</i> -indacene)] ²⁺ {[BF ₄] ⁻ } ₂ , 3a²⁺	2	4.16	1.5
Cp* ₂ Co ₂ (<i>as</i> -indacene), 3b	2	2.51, 2.72	10.4, -7.56
[Cp* ₂ Co ₂ (<i>as</i> -indacene)] ⁺ [BF ₄] ⁻ , 3b⁺	1	1.56	-6.63
Cp* ₂ Ni ₂ (<i>as</i> -indacene), 3c (not CW)	4	see text	
[Cp* ₂ Ni ₂ (<i>as</i> -indacene)] ⁺ [BF ₄] ⁻ , 3c⁺	3	2.35	-82

^a Diamagnetic corrections used: indacene, -99×10^{-6} emu/mol; pentalene, -66×10^{-6} emu/mol; [BF₄]⁻, -32.2×10^{-6} emu/mol; FeCp*₂, -120×10^{-6} emu/mol; FeCp*₂, -120×10^{-6} emu/mol; CoCp*₂, -120×10^{-6} emu/mol; NiCp*₂, -122×10^{-6} emu/mol; and RuCp*₂, -133×10^{-6} emu/mol.

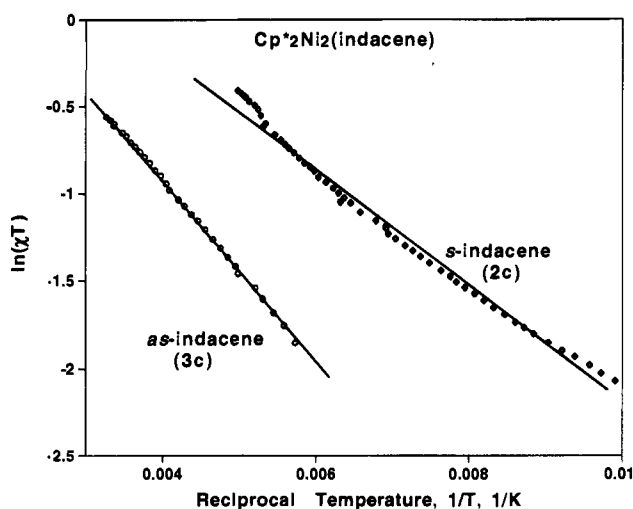


Figure 3. Fit of the magnetic susceptibility data for **2c** and **3c** to eq 2.

These low-energy absorbances were not observed for the neutral or the dicationic forms, although occasionally neutral **1c** exhibited a weak absorbance at 1007 nm (9930 cm^{-1}). This was attributed, however, to adventitious oxidation of this compound. The spectra were obtained in CD₂Cl₂ to minimize solvent contributions from C-H overtones in CH₂Cl₂. This was especially important for the exceptionally low energy transitions observed for the iron complexes **1a⁺** and **2a⁺**. According to Hush,¹⁸ the thermal energy required for electron transfer for a symmetrically substituted bimetallic complex can be estimated from the energy of the optical transition by $E_{\text{th}} \sim E_{\text{op}}/4$, where $E_{\text{op}} = h\nu_{\text{max}}$. Decreasing values of $h\nu_{\text{max}}$ correspond to a smaller

(18) Hush, N. S. *Prog. Inorg. Chem.* **1967**, *8*, 391.

Table 6. ⁵⁷Fe Mössbauer Parameters for Pentalene and Indacene Bridged Complexes

	temp, T (K)	isomer Shift, ^a δ (mm/s)	quadrupole splitting, ΔE (mm/s)
Cp* ₂ Fe ₂ (pentalene), 1a	293	0.48	2.49
[Cp* ₂ Fe ₂ (pentalene)] ⁺ [BF ₄] ⁻ , 1a⁺	77	0.52	2.51
[Cp* ₂ Fe ₂ (pentalene)] ²⁺ {[BF ₄] ⁻ } ₂ , 1a²⁺	293	0.43	1.31
	4.2	0.41	1.30
	293	0.38	0.74
	4.8	0.54	0.80
Cp* ₂ FeRu(pentalene), 1e	293	0.43	2.55
[Cp* ₂ FeRu(pentalene)] ⁺ [BF ₄] ⁻ , 1e⁺	77	0.56	2.51
	293	0.42	0.97
	77	0.54	0.99
	4.8	0.54	0.99
Cp* ₂ FeCo(pentalene), 1f	77	0.51	2.33
[Cp* ₂ FeCo(pentalene)] ⁺ [BF ₄] ⁻ , 1f⁺	77	0.51	2.29
[Cp* ₂ FeCo(pentalene)] ²⁺ {[BF ₄] ⁻ } ₂ , 1f²⁺	77 ^b	0.52	0.94
Cp* ₂ Fe ₂ (<i>s</i> -indacene), 2a	77	0.49	2.40
	4.2	0.46	2.30
	1.5	0.47	2.30
[Cp* ₂ Fe ₂ (<i>s</i> -indacene)] ⁺ [BF ₄] ⁻ , 2a⁺	293	0.47	1.64
	4.8	0.55	1.67
	1.5	0.57	1.68
Cp* ₂ Fe ₂ (<i>as</i> -indacene), 3a	293	0.54	2.60
	77	0.55	2.60
[Cp* ₂ Fe ₂ (<i>as</i> -indacene)] ⁺ [BF ₄] ⁻ , 3a⁺	293	0.42	0.39
		0.43	2.07
	77	0.49	0.43
		0.50	2.29

^a mm/s vs natural iron. ^b Impurity background doublet: $\delta = 0.50$ mm/s and $\Delta E = 2.29$ mm/s.

thermal barrier to electron transfer and a greater effective thermal electron transfer rate constant, k_{th} . The ΔE values in Table 2 determined from cyclic voltammetry generally are taken as an indication of the extent of delocalization; larger values of ΔE

are tantamount to larger values of k_{th} . Therefore, $h\nu_{max}$ should vary inversely with ΔE . Indeed, the ΔE values for the symmetrical complexes **1a–c** correlate with $h\nu_{max}$ in the expected manner. However, this correlation is not apparent for the remaining complexes. The peak widths at half-height, $\Delta h\nu_{1/2}$, for all the complexes are significantly less than that predicted by Hush¹⁸ for symmetrical one-electron transfer, in which $\Delta h\nu_{1/2} = (2.31h\nu_{max})^{1/2}$. In addition, the $h\nu_{max}$ values are essentially independent of the dielectric properties of the solvent; for all complexes $h\nu_{max}$ values in propylene carbonate were <1% greater than in CD₂Cl₂. The spectral features for the symmetrical monocationic complexes are consistent with strong coupling between metal centers and with a valence delocalized description. The value of k_{th} can be estimated from eq 1, provided the entropy of activation is assumed to be zero.^{2b} The values of k_{th} estimated in this manner for the mixed-valent complexes range from 10⁹ to 10¹⁰ s⁻¹, which are characteristic of a fully delocalized system (Class III).¹⁷

$$k_{th} \approx \frac{k_B T}{h} \exp\left(-\left[\frac{E_{op} - RT}{4 RT}\right]\right) \quad (1)$$

Inspection of Table 4 reveals that the values of $h\nu_{max}$ are appreciably different for the different complexes. This is not unreasonable considering the changes in orbital occupation in the series **1a–1c**. The distortions accompanying intervalent transfer in **1a**⁺ are not expected to be large since this involves a d⁵–d⁶ system. On the other hand **1b**⁺ (d⁶–d⁷) and **1c**⁺ (d⁷–d⁸) involve antibonding orbitals and intervalent electron transfer would be expected to be accompanied by a greater degree of distortion. The optical properties of the mixed-valent heterometallic complexes are similar to those of the homometallic ions, consistent with localization of the optical transition on one of the metal centers.

Magnetic Properties. The different molecular structures of the pentalene and *s*- and *as*-indacene ligands offer a unique opportunity to examine the role of ligand symmetry on the magnetic properties of their complexes, and the spins/dimer, room temperature effective magnetic moments, and fits of the susceptibility (χ) to the Curie–Weiss expression, $\chi \propto (T - \theta)^{-1}$, are summarized in Table 5. Small decreases of the magnetic moment (0.2 to 0.4 μ_B) over the decreasing temperature range of 298 to 4.2 K were observed, consistent with depopulation of higher lying spin orbit states. Based on the crystal structures, intermolecular exchange is expected to be weak and typically antiferromagnetically coupled as evidenced from the observed negative θ -values. Indeed, there is no evidence of cooperative magnetic behavior for any of the systems.

The systems with one spin per complex exhibit the expected magnetic moments. The moments for the iron-containing complexes are variable and generally higher than that predicted for a spin only value of 1.73 μ_B (with $g = 2$). This is attributed to the highly anisotropic g -values associated with the ferrocene-like centers (vide infra) and classical orbital contributions to the moment. Cp*₂FeCo(pentalene) (**1f**) has a room temperature moment of 1.79 μ_B consistent with that of the unpaired electron residing on the Co^{II} and diamagnetic low-spin Fe^{II}. In contrast, oxidation to the dication **1f**²⁺ results in the unpaired electron residing on the Fe^{III}, which due to its highly anisotropic g values has a larger moment of 2.43 μ_B . Similarly, the 1.90 μ_B moment for [Cp*₂FeRu(pentalene)]⁺ (**1e**⁺) suggests the presence of an unpaired spin on an iron center. The moments for monocationic dicobalt indacene salts **2b**⁺ and **3b**⁺ are comparable to each other, *i.e.*, 1.59 ± 0.03 μ_B , but unexplainably slightly lower than the expected $g = 2$ spin only value of 1.73 μ_B . Indeed, this ideal μ_B value is only observed for **1b**⁺. Complexes **1a**,

1d, **1e**, **1b**²⁺, **1f**²⁺, **2a**, **2b**²⁺, **3a**, and **3a**²⁺, which are predicted to have no unpaired electrons, are diamagnetic, although a few samples had susceptibilities characteristic of doublet spin impurities.

Several of the complexes reported here may have two or more spins based on simple electron counting. These spins may intramolecularly couple ferromagnetically or antiferromagnetically, leading to triplet or singlet states, respectively. The neutral dicobalt complexes **1b** and **2b** and dicationic dinickel salt **1c**²⁺, which ostensibly have one unpaired electron per metal site by the electron counting formalism,¹⁹ are diamagnetic. This is consistent with a singlet ground state arising from intramolecular antiferromagnetic coupling. Antiferromagnetic coupling is also evident for the monocation dinickel complexes **1c**⁺, **2c**⁺, and **3c**⁺, which each ostensibly possess three unpaired spins, with moments ranging from 1.69 to 2.35 μ_B . In contrast, ferromagnetic coupling is suggested by the high moment observed for the neutral dicobalt *as*-indacene complex, **3b**, and dicationic dinickel complex, **2c**²⁺ (2.61 and 2.01 μ_B , respectively). In addition, the dication diiron complexes **1a**²⁺, **2a**²⁺, and **3a**²⁺ all exhibit high moments, characteristic of ferromagnetic coupling. The susceptibility of the diiron *s*-indacene complex **2a**²⁺ is unusual as it cannot be parametrized by a single Curie–Weiss expression between 4 and 300 K; above 100 K it can be fit with $\theta = -37$ K and below 100 K to $\theta = -1.6$ K. This suggests that diiron(III)-based oligomers will also be ferromagnetically coupled and that sufficiently long oligomers/polymers based on these building blocks might exhibit magnetic ordering.

The neutral dinickel complexes have a pair of triplet Ni(II) sites which can couple antiferromagnetically or ferromagnetically, leading to limiting singlet or quintet states, respectively. The pentalene complex **1c** is diamagnetic, consistent with antiferromagnetic coupling. In contrast, the indacene-based salts (**1b** and **1c**) have moments of 2.97 and 2.61 μ_B , respectively, suggesting $S = 1$ triplet ground states. Susceptibility data for **2c** can be fit to the Curie–Weiss expression between 4 and 50 K, but at ~60 K the susceptibility exceeds that expected from Curie-like behavior. At 210 K, the susceptibility exhibited a sharp transition, followed by a decrease in susceptibility with increasing temperature. This behavior suggests the presence of a triplet excited state. Fitting the data to the Bleaney–Bowers equation, eq 2, while taking account of possible free-spin impurities resulted in a singlet–triplet gap, $\Delta\epsilon_{S-T}$, of 0.036 eV (290 cm⁻¹; 0.83 kcal/mol) with a 10% doublet impurity, Figure 3. We view this interpretation with caution, however, as the data do not conform to the Bleaney–Bowers behavior at high temperature. Rather, the abrupt change in susceptibility observed at 210 K suggests a phase transition. The moment per metal ion at high temperature was 3.40 μ_B . The moment expected for four independent $S = 1/2$ spins is 3.46 μ_B , while that expected for two $S = 1$ centers is 4.0 μ_B . While we cannot explain the magnetic behavior definitively, the formally $S = 1$ Ni centers appear to be significantly coupled.

$$\chi = [g^2 N \mu_B^2 / k_B T] / [3 + \exp(-\Delta\epsilon_{S-T} / k_B T)] \quad (2)$$

Magnetic susceptibility measurements of **3c** also indicate the presence of a singlet ground state and a higher spin excited state, Figure 3. The data gave the best fit for $\Delta\epsilon_{S-T}$ of 0.056 eV (524 cm⁻¹, 1.29 kcal/mol) with an 11% doublet impurity. The higher energy gap observed for **3c** compared to **2c** appears to indicate more extensive antiferromagnetic coupling in the former.

⁵⁷Fe Mössbauer Spectroscopy. Homobinuclear Systems. The ⁵⁷Fe Mössbauer spectra of the homobinuclear iron com-

(19) We have adopted an electron counting formalism here that treats the ligands as anions and the metal centers as Ni^{II} ions.

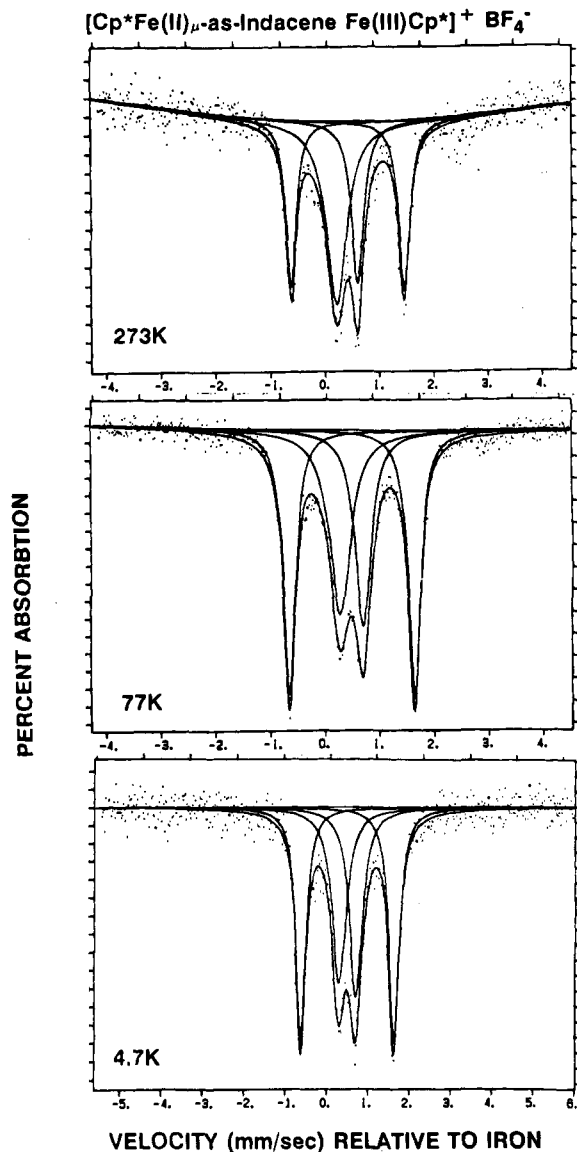


Figure 4. Mössbauer spectra of $[\text{Cp}_2^*\text{Fe}_2(\text{as-indacene})]^{+}$ (3a^+).

plexes bridged by *s*- and *as*-indacene ligands have been reported elsewhere²⁰ for the neutral and monocationic materials. (The dicationic forms have not been isolated for these bridging ligands.) The neutral analogs exhibit large (values ranging from ~ 2.2 to ~ 2.6 mm/s), essentially temperature independent quadrupole splitting (ΔE) effects reminiscent of ferrocene and decamethylferrocene.²¹ 2a^+ exhibits a single intermediate value (Table 6) quadrupole doublet and appears to be completely valence detrapped on a ^{57}Fe Mössbauer time scale (*i.e.*, electron transfer rates $> 10^7$ s $^{-1}$) to as low as 1.5 K. At this temperature $k_{\text{B}}T \sim 1$ cm $^{-1}$, thus any energy barrier to intramolecular electron transfer is effectively zero. The monocationic *as*-indacene complex exhibits classical trapped ferrocene and ferrocenium centers ($I_{\text{Fe}^{\text{II}}}/I_{\text{Fe}^{\text{III}}} \approx 1$ at 4.2 K), Figure 4, with evidence of incipient detrapping behavior only at ambient temperature. This contrasts strongly with the corresponding unmethylated cyclopentadiene analog $[\text{CpFe}^{\text{II}}\mu\text{-as-indaceneFe}^{\text{III}}\text{Cp}]^+\text{I}_3^- \cdot 0.5\text{I}_2$ which exhibits gradual detrapping and essential averaging over the

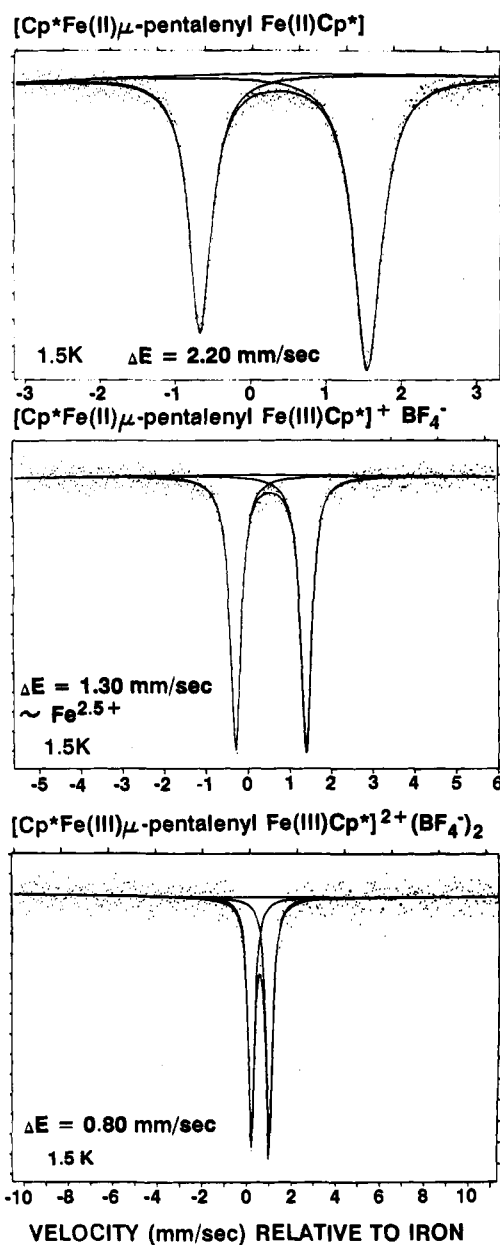


Figure 5. Mössbauer spectra of $[\text{Cp}_2^*\text{Fe}_2(\text{pentalene})]^n$ ($n = 0, 1+, 2+$), 1a , 1a^+ , 1a^{2+} .

increasing temperature range of 100–300 K.²² This was correlated with an activation energy (δ) for electron hopping of ~ 0.04 eV (~ 325 cm $^{-1}$). The origin of the apparently higher value of δ for the permethylated $(\text{Cp}^*)\text{-}\mu\text{-as-indacene}$ complex is not clear. It may be related to differences in counter anion $\{[\text{BF}_4]^- \text{ vs } \text{I}_3^-\}$ rather than specific ligation (Cp vs Cp*). A better understanding of these systems should arise from the detailed investigation of counterion effects as well as a study of $[\text{Cp}^*\text{Fe}^{\text{II}}\mu\text{-as-indaceneFe}^{\text{III}}\text{Cp}]^+[\text{BF}_4]^-$, *i.e.*, the “half” permethylated analog.²²

Fortunately, all three members of the pentalene bridged series $[\text{Fe}^{\text{II/III}}]^\circ$, $[\text{Fe}^{\text{II/III}}]^{+}$, and $[\text{Fe}^{\text{II/III}}]^{2+}$ have been isolated as pure solids. Their Mössbauer spectra at 1.5 K are shown in Figure 5. The extremes of ferrocene (low spin Fe^{II}) and ferrocenium (low spin Fe^{III}) are evident for the neutral and dicationic complexes. The monocation is fully detrapped to as low as 1.5 K and exhibits a unique environment in a highly delocalized binuclear system. As perhaps expected, the observed value of

(20) Reiff, W. M.; Manriquez, J. M.; Ward, M. D.; Miller, J. S. *Mol. Cryst., Liq. Cryst.* **1989**, *176*, 423.

(21) Greenwood, N. N.; Gibbs, T. C. *Mössbauer Spectroscopy*; Chapman and Hall, Ltd.: London, UK, 1971.

(22) $[\text{Cp}^*\text{Fe}^{\text{II}}\mu\text{-as-indaceneFe}^{\text{III}}\text{Cp}]^+[\text{TCNE}]^{+}$ also exhibits detrapping effects for $300 > T > 100$ K: Reiff, W. M.; Rreis, J.; Kirss, R., unpublished results.

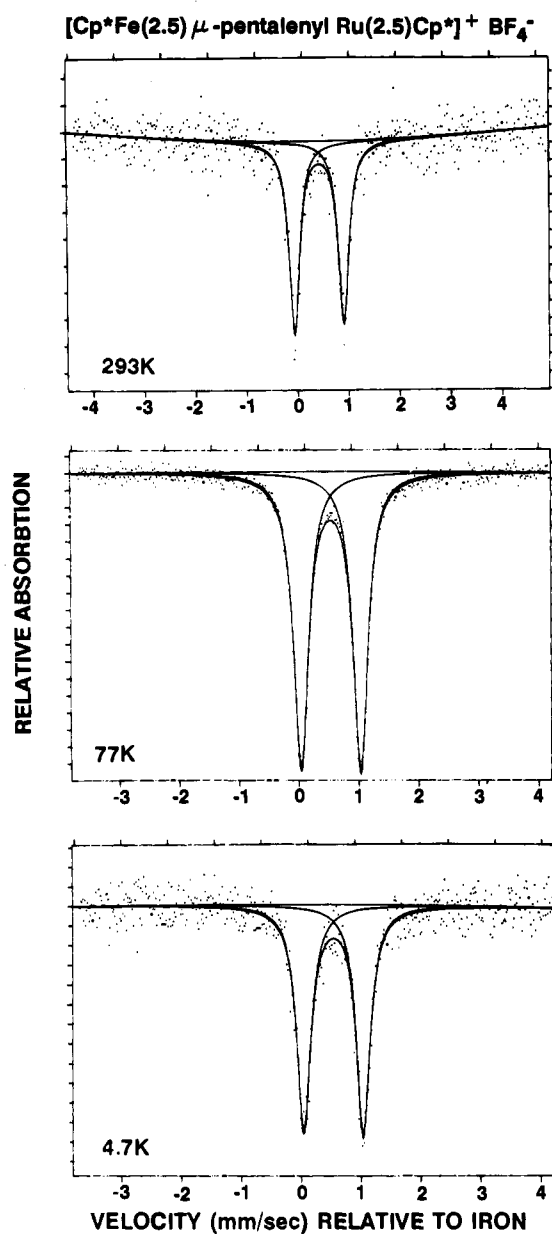


Figure 6. Mössbauer spectra of $[\text{Cp}_2^*\text{FeRu}(\text{pentalene})]^{2+}$ as a function of temperature.

the quadrupole splitting for the monocation is reasonably close to the simple average (1.50 mm/s) of those for the neutral and dicationic systems. The observed Mössbauer spectra reflect solid-state electron transfer rates of $>10^7 \text{ s}^{-1}$. (The ^{57}Fe $I = 3/2$ excited state lifetimes are of order 100 ns.)²¹

Heterobinuclear Systems. The $[\text{Cp}^*\text{Fe}-\mu\text{-pentaleneM}\text{Cp}^*]^n$ [$M = \text{Ru}$ ($n = 0, 1+$); Co ($n = 0, 1+, 2+$)] heterobinuclear systems have also been characterized by Mössbauer spectroscopy. Again the ^{57}Fe Mössbauer spectra indicate a unique averaged iron environment for the monocationic Ru system over the entire range 1.5–300 K (Figure 6), *i.e.*, a completely detrapped system. A $(\text{Fe}^{\text{II}}, \text{Ru}^{\text{III}}) \rightarrow (\text{Fe}^{\text{III}}, \text{Ru}^{\text{II}})$ transition is reported as the temperature is increased from 78 K to ambient for the dimethylene bridged [1.1]-ferrocenylruthenocenophane monocation.²³ A possible reason for the different behaviors of these $(\text{Fe}, \text{Ru})^+$ systems is the fused nature of the pentalenyl bridge considered herein vs coupling via $-\text{CH}_2-$ groups and perhaps differing packing effects.²³ It seems clear that any rotation about the latter will change the degree of metal–metal interaction and/or electron delocalization.

(23) Watanabe, M.; Sano, H. *Bull. Chem. Soc. Jpn. Lett.* 1988, 1457.

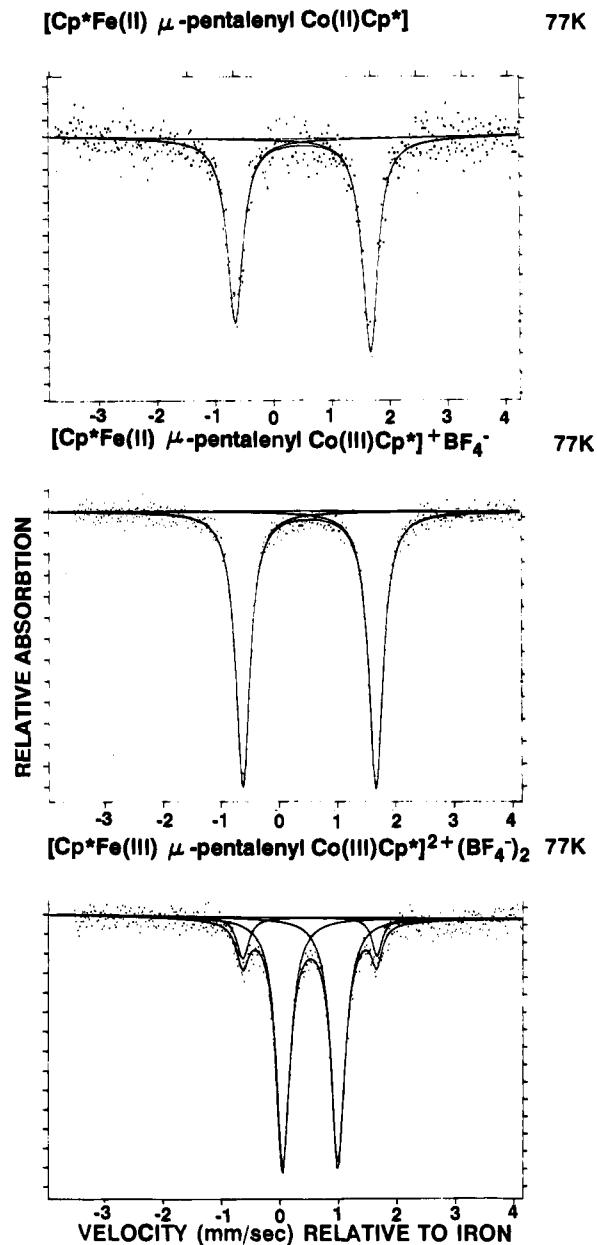


Figure 7. Mössbauer spectra of $[\text{Cp}_2^*\text{FeCo}(\text{pentalene})]^n$ ($n = 0, 1+, 2+$) at 77 K.

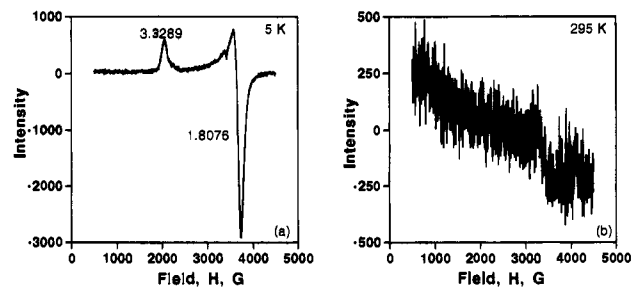


Figure 8. EPR spectra of $[\text{Cp}_2^*\text{Fe}_2(\text{as-indacene})]^+ [\text{BF}_4]^- (3\text{a}^+)$ at 5 K (a) and 295 K (b).

The Mössbauer spectrum of the neutral Fe/Co system corresponds to “ferrocene”-like behavior with the electron spin residing on the low-spin Co^{II} . Interestingly, the Mössbauer spectrum of the monocation is also like that of ferrocene (Figure 7). This attests to the great stability of the diamagnetic, low-spin d^6 configuration of Co^{III} . That is, the oxidation of the neutral heterocomplex to the monocation corresponds to loss of an electron from the spin doublet Co^{II} center and little if any perturbation of iron centers. Finally, the formation of the

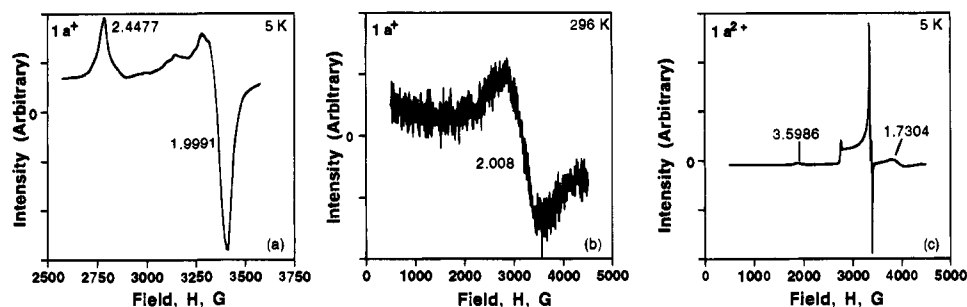


Figure 9. EPR spectra of $[Cp_2^*Fe_2(pentalene)]^+ \{ [BF_4]^- \}$ ($1a^+$) at 5 (a) and 296 K (b) and $[Cp_2^*Fe_2(pentalene)]^{2+} \{ [BF_4]^- \}_2$ ($1a^{2+}$) at 5 K (c).

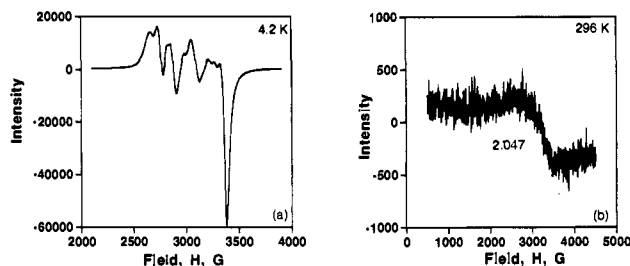


Figure 10. EPR spectra of $[Cp_2^*FeRu(pentalene)]^+ \{ [BF_4]^- \}$ ($1e^+$) at 4.2 (a) and 296 K (b).

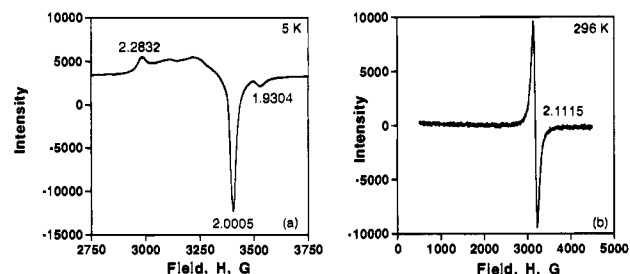


Figure 11. EPR spectra of $[Cp_2^*Fe_2(s-indacene)]^+ \{ [BF_4]^- \}$ ($2a^+$) at 5 (a) and 296 K (b).

dication is expected to involve loss of an electron by Fe^{II} to give Fe^{III} , again consistent with the observed Mössbauer spectrum and EPR data and the expected redox behavior of the MCp^* fragment. The lower-intensity background doublet of the dications spectrum undoubtedly is due a ferrocene-like impurity arising from the incomplete oxidation of $Cp^*Fe-\mu-pentaleneCoCp^*$. We also note that the temperature dependencies of the magnetic susceptibilities and magnetic moments for the $\{Fe-Co\}$ system agree with the spin assignments.

Electron Paramagnetic Resonance. The application of varying time scale techniques is clearly required in order to distinguish between the alternatives for electron exchange between metal sites in these bimetallic systems for averaging via thermal activation over a barrier between vibronic states, *i.e.*, quantum mechanical tunneling between such states, or complete delocalization.

For the valence trapped versions of the systems under consideration, one anticipates a combination of diamagnetic low-spin Fe^{II} (EPR silent) and low-spin Fe^{III} , where the latter usually exhibits a high degree of g -factor anisotropy.²⁴ With valence detrapping and/or significant delocalization for the low-spin iron systems discussed herein, the EPR signals become progressively more isotropic with the approach to an averaged state, as observed in the EPR spectra of these complexes (Figures 8–11, Table 7). The spectrum of the monocationic *as*-indacene complex $3a^+$ (Figure 8) is characteristic of classical low-spin (ferrocenium) Fe^{III} with $\Delta g = |g_{||} - g_{\perp}| = 1.52$, consistent with the valence-trapped low-spin Fe^{III} indicated by the Mössbauer

Table 7. Principle g -Values for Selected Iron-Containing Pentalene and Indacene Complexes

complex	temp <i>T</i> , K	<i>g</i> -values
$[Cp_2^*Fe_2(pentalene)]^+ \{ [BF_4]^- \}$, $1a^+$	5	2.4477, 1.9991
$[Cp_2^*Fe_2(pentalene)]^{2+} \{ [BF_4]^- \}_2$, $1a^{2+}$	5	3.5986, 2.4417, 2.0199, 1.9898, 1.7054
$[Cp_2^*Co_2(pentalene)]^+ \{ [BF_4]^- \}$, $1b^+$	5	2.0776, 2.0262, 1.9703, 1.9479, 1.9247
$Cp^*FeCo(pentalene)$, $1f$	4.2	2.1080, 2.0037, 1.9542
$[Cp_2^*FeCo(pentalene)]^{2+} \{ [BF_4]^- \}_2$, $1f^{2+}$	4.2	4.0446, 2.4695, 2.0176, 1.9916, 1.7586
$[Cp_2^*FeRu(pentalene)]^+ \{ [BF_4]^- \}$, $1e^+$	4.2	2.5331, 2.4426, 2.3374, 2.2573, 2.1826, 2.0958, 2.0630, 1.9896
$[Cp_2^*Fe_2(s-indacene)]^+ \{ [BF_4]^- \}$, $2a^+$	5	2.2832, 2.0005, 1.9304
$[Cp_2^*Co_2(s-indacene)]^+ \{ [BF_4]^- \}$, $2b^+$	5	2.01455, 1.9662
$[Cp_2^*Fe_2(as-indacene)]^+ \{ [BF_4]^- \}$, $3a^+$	5	3.3289, 1.8076
$[Cp_2^*Co_2(as-indacene)]^+ \{ [BF_4]^- \}$, $3b^+$	5	1.9433

spectra. This contrasts strongly with $1a^+$ and $2a^+$ complexes (Figures 9, 11) for which Δg is only 0.45 and 0.35, respectively. On the other hand, the EPR spectrum of $1a^{2+}$ (Figure 9c) reflects equivalent, highly anisotropic ($\Delta g = 1.87$) low-spin Fe^{III} environments.

The 4.2 K EPR spectra of the heterobinuclear systems likewise are consistent with their respective Mössbauer spectra. The spectrum of $1f$ is that expected for spin doublet ground state Co^{II} while that of $1f^+$ is EPR silent, as expected for low-spin Fe^{II} and Co^{III} . $1f^{2+}$ exhibits large anisotropy ($\Delta g = 2.28$) as expected for the ferrocenium Fe^{III} . In contrast, the spectrum of $[1e^+][BF_4]^-$ (Figure 10a) reflects a significantly reduced g -factor anisotropy ($\Delta g = 0.54$) again corresponding to valence detrapping as suggested by its Mössbauer spectra. This spectrum is also complicated by hyperfine splitting which is not considered further.

For low-spin Fe^{III} [whether $^2T_{2g}$ (O_h) or axially distorted], the EPR spectra are typically highly broadened and often unobservable at ambient temperature owing to significant spin lattice relaxation effects.²⁴ The relaxation effects are a direct function of the degree of the unquenched orbital angular momentum (*i.e.*, $L \neq 0$) for the ground electronic state of the system. This behavior is clearly reflected by a barely observable highly broadened signal in the ambient temperature spectrum of the trapped Fe^{III} species in $3a^+$ (Figure 8b). In contrast, relaxation broadening effects related to orbital angular momentum should be mitigated by the admixture of 1A (of low-spin Fe^{II}) into the system ground state, with a concomitant reduction in the value of Δg . The result of the detrapping process leads to the expectation of "observable" EPR spectra even at ambient temperature. The detrapped iron systems of this study exhibit

(24) Prins, R. *Mol. Phys.* 1970, 19, 603.

this effect with the $2\mathbf{a}^+$ as a spectacular example (Figure 11b) versus $3\mathbf{a}^+$, Figure 8b. Our use of EPR (Zeeman state lifetimes $\sim 10^{-9}$ to 10^{-10} s) in the present context establishes solid-state electron transfer rates of order 10^{10} s^{-1} for certain of the monocationic complexes consistent with the values estimated from the mixed valent optical transitions observed in the near-IR spectral region.

Conclusion

The magnetic susceptibility, X-ray crystallographic, electrochemical, and spectroscopic studies of $[\text{Cp}^*\text{M}(\text{ligand})\text{M}'\text{Cp}^*]^n$ ($\text{M}, \text{M}' = \text{Fe}, \text{Co}, \text{Ni}; n = 0, 1+, 2+$; ligand = pentalene, *s*-indacene, *as*-indacene) reveal delocalized strong electron coupling between metal sites. This coupling results in large electrochemical potential separations between successive one-electron redox events and varying degrees of intramolecular ferromagnetic or antiferromagnetic coupling between metal centers containing (formally) unpaired spins. The mixed-valent ($n = 1+$) complexes exhibit intervalent charge transfer absorption bands. Due to the delocalization and strong coupling between metal centers, oligomers an/or polymers containing μ_2 -bridging pentalene and *s*-indacene ligands might have novel electrical and magnetic, including cooperative magnetic, proper-

ties. Synthetic strategies are currently being devised and pursued in this context.

Acknowledgment. W.M.R. gratefully acknowledges support from the NSF DMR Materials Research Program and the donors of the Petroleum Research Fund, administered by the American Chemical Society. We appreciate the technical assistance provided by Carlos Vazquez, Daniel Wipf, William Marshall, Richard L. Harlow, R. Scott McLean, Ray Richardson, Edward Delawski, Fred Davidson, and Derrick Ovenall.

Supplementary Material Available: A summary of the crystallographic data, atom labeling diagrams, tables of fractional coordinates, bond distances and angles, least-square plane, anisotropic thermal parameters, general displacement parameters for $1\mathbf{b}$, $[1\mathbf{a}^+]\text{BF}_4^-$, $[\text{Cp}^*\text{Fe}(\text{pentalene})\text{Cp}^*]^+[\text{BF}_4]^-$, $2\mathbf{a}$, $2\mathbf{c}$, $[2\mathbf{c}^+]\text{BF}_4^- \cdot \text{CH}_2\text{Cl}_2$, $[2\mathbf{a}^+]\text{BF}_4^-$, $[2\mathbf{b}^{2+}][\text{BF}_4^-]_2$, and $3\mathbf{a}$ (89 pages); tables of calculated and observed structure factors (78 pages). This material is contained in many libraries on microfiche, immediately follows this article in the microfilm version of the journal, can be ordered from the ACS, and can be downloaded from the Internet; see any current masthead page for ordering information and Internet access instructions.

JA9500116